

Cloud Coverage Disruption for Groundwater Recharge Improvement Using Remote Sensing Techniques in Asir Region, Saudi Arabia

Mohamed Elhag* and Jarbou Bahrawi

Department of Hydrology and Water Resources Management, Faculty of Meteorology, Environment and Arid Land Agriculture, King Abdulaziz University, P.O. Box 80208 Jeddah 21589 Saudi Arabia

melhag@kau.edu.sa

Abstract: Remote sensing technology have showed robust capacities in meeting challenges of water resource management, in the countries like kingdom of Saudi Arabia where rapid population growth is imposing stress on scarce water resources. Also, continual Earth observations from space are important to manage water resources for the benefit of humankind and the environment, as well provide important forecasting services to prevent water-related disasters such as floods and droughts. Remote sensing approaches to assess and manage of water resources are important especially in the region of Saudi Arabian because no satisfactory hydrological networks exist. Cloud detection is important issue in extracting information of geophysical, geomorphological and meteorological interest from remotely sensed images. Present work aimed at imposing a new method for cloud detecting and producing cloud probability mapping of multispectral images acquired using MERIS images. The algorithm was implemented on 59 satellite imageries collected from January 2006 to October 2011.

[Mohamed Elhag and Jarbou Bahrawi. **Cloud Coverage Disruption for Groundwater Recharge Improvement Using Remote Sensing Techniques in Asir Region, Saudi Arabia.** *Life Sci J* 2014;11(1):192-200]. (ISSN:1097-8135). <http://www.lifesciencesite.com>. 29

Keywords: Classification, Cloud Detection, Cloud Probability, MERIS, Remote Sensing, Water Resources Management

1. Introduction

Water cycle is all about storing water and moving water on, in, and above the Earth. Although the atmosphere may not be a great storehouse of water, it is the superhighway used to move water around the globe. There is always water in the atmosphere. Clouds are, of course, the most visible expression of atmospheric water, but even clear air contains water in particles that are too small to be seen. One estimate of the volume of water in the atmosphere at any one time is about 12,900 km³. That may sound like a lot, but it is only about 0.001 percent of the total Earth's water volume.

Clouds exert a dominant influence on solar energy absorbed by the Earth and on infrared radiation emitted to space. It is known that clouds present a problem they act to cool the planet by reflecting solar radiation to space and warm the planet by reducing radiation emitted to space [1; 2; 3]. Accurate detection of clouds from remote sensing images is with a major concern for a wide range of remote sensing applications, especially by sensors detecting ultraviolet (UV) and visible and near-infrared (VNIR) range of the electromagnetic spectrum [4; 5].

Cloud screening involves discriminating between clear and cloudy pixels in an image. Reviews of cloud detection methods can be found in Goodman and Henderson-Sellers [3], Rossow [6] and Rossow *et al.* [7]. Methods for identifying clouds are based on radiance threshold, radiative transfer model, or

statistical techniques making use of spectral and textural features in the imagery. Radiance threshold techniques work monthly, and single or multiple-channel thresholds are defined which are then used to divide clear and cloudy pixels. Radiative transfer model techniques use one or more spectral radiance measurements as input to an atmospheric radiative transfer model and retrieve a physical quantity such as cloud optical thickness or altitude. Pixels are then determined to be clear or cloudy based on thresholds in the retrieved quantity. Statistical techniques use groups of adjacent pixels. Among these are methods based on spatial coherency between adjacent pixels [8] artificial neural networks [9], maximum likelihood decision rules [10], and clustering routines [11]. Specific cloud detection algorithms applied to satellite data have features which are worthwhile for a particular scene class [12].

In particular, performance of the presented approach is tested on images from recent multispectral instrument with the following characteristics: the Medium Resolution Imaging Spectrometer (MERIS) instrument on board the European Space Agency (ESA) ENVISAT environmental satellite. Two of the key features of the MERIS instrument are its temporal resolution (revisit time of 3 days) and its spatial coverage (swath width of 1150 km), which make unavoidable the presence of cloud covers. In Reduced Resolution (RR), MERIS provides 1000 m pixel-size images with 15 narrow bands, in the spectral range

from 400 nm to 1000 nm, at unprecedented spectral and radiometric resolutions [13]. For further details see Brockmann *et al.* [14].

The aim of the current study is to examine the spatiotemporal distribution of the conducted cloud likelihood maps over the Southern part of KSA using MERIS data collected from January 2006 till October 2011.

2. Material and Methods

2.1. Study area

Asir region is located at the southwestern Saudi Arabia (Figure 1). Asir consists of about 100,000 km² of Red Sea coastal plains, high mountains, and the upper valleys of the wadis (seasonal watercourses) are Bīshah and Tathlīth. Asir is a prosperous agricultural region. It has an area of 77,088 km² and an estimated population of 1,563,000. It shares a short border with Yemen. Its capital is Abha. The average annual rainfall in the highlands probably ranges from 300 to 500 mm falling in two rainy seasons, the chief one being in March and April with some rain in the summer. Temperatures are extreme, with diurnal temperature ranges in the highlands the greatest in the world. It is common for afternoon temperatures to be over 30 °C, yet mornings can be frosty and fog can cut visibility to near zero percent. As a result, there is much more natural vegetation in Asir than in any other part of Saudi Arabia.

2.2. Cloud probability

2.2.1. Algorithm specification

The cloud probability algorithm has been developed and performed by Free University Berlin and Brockmann Consult. It is also used in the Global MERIS Land Albedo map project [13]. The cloud probability algorithm is using nine spectral bands of MERIS. Specifically, the ratio of band 10 (Cloud optical thickness, cloud-top pressure reference), band 11 (Cloud-top / Surface pressure) and band 12 (Aerosol, vegetation) which is an indication of the absorption due to oxygen, the European Center for Medium-Range Weather Forecasts (ECMWF) surface pressure and the exact wavelength of band 11 as input. As an output, it yields a probability value (0 to 1) pointing out if a pixel can be regarded as a cloud or not. Such a probability permits a more flexible way to work with identified clouds compared to a binary cloud mask.

The algorithm uses two different artificial neural nets. The first one is used over the open ocean and the second one overland. The distinction between ocean and land is done using the altitude information. If the altitude is lower than 50 meters then, the ocean Artificial Neural Network is not used and the land Artificial Neural Network is implemented like the current study.

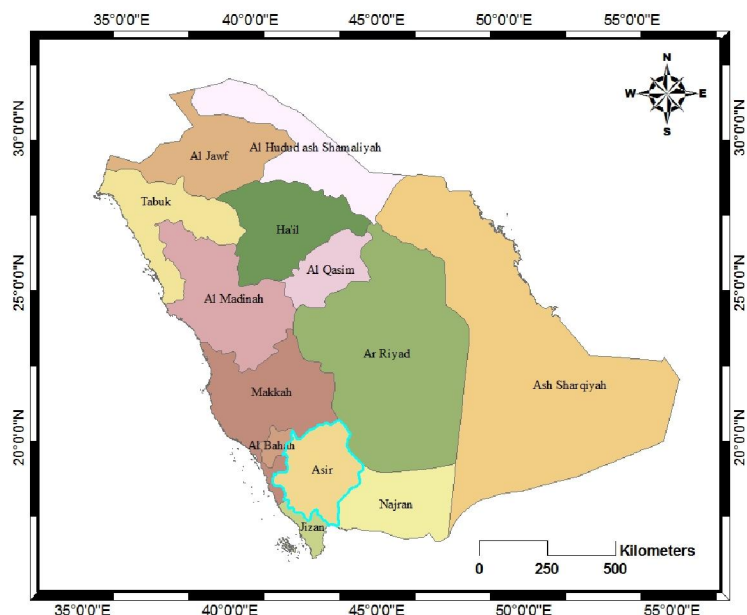


Figure 1, Administrative boundaries of KSA regions with location of the study area highlighted

The following Figure 2 shows the general structure of the cloud detection algorithm. During development of the algorithm by Fischer and Grassl [14]; Fell and Fischer [15], using the radiative transfer

model MOMO (Matrix Operator Method), simulated cloud and noncloud top of atmosphere radiance have been produced and an Artificial Neural Net has been trained. Thus, Artificial Neural Network is now used in

the Cloud Probability Processor, where it is fed with the reflectances and the pressure as shown in the Figure 2. A post-processing is applied after the net (nn2prop)

which scales the output of the Artificial Neural Network into a probability value.

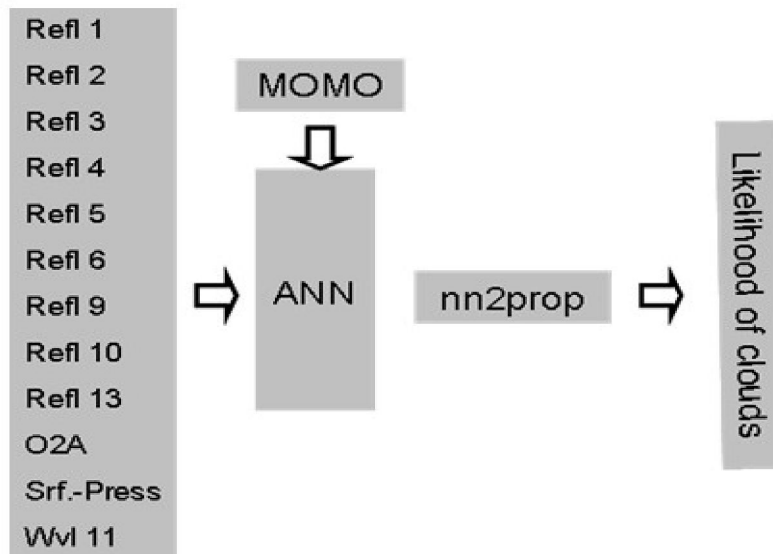


Figure 2, Cloud detection algorithm.

2.2.2. Algorithm basics

According to Lindstrot *et al.* [17], clouds are easily to detect when a manual classification of satellite images is done, their automatic detection is difficult. Clouds have four special radiative properties that enable their detection: 1) clouds are white, 2) clouds are bright, 3) clouds are higher than the surface and 4) clouds are cold. However clouds, as the most variable atmospheric constituent, seldom show all four properties at the same time.

Thin clouds show a portion of the underlying surface spectral properties, and low clouds are sometimes warm. Also, some surface types like snow and ice have spectral properties that are similar to some of the cloud properties. Therefore simple thresholding algorithms often fail, and existing cloud detection schemes use several different cascaded threshold based tests to account for the complexity [18; 19; 20].

2.2.3. Algorithm specification

In general, cloud detection algorithms can be separated into two classes: clear sky conservative and cloud conservative. Clear sky conservative algorithms are constructed such the probability of a first order error in clear sky detection is low; in other words: if a pixel is detected as clear the probability of cloudiness should be low [21]. This often has the side effect that many cloud free pixels are detected as cloudy. The opposite is true for cloud conservative algorithms. Here the probability of a first order error in cloud detection is low, with the side effect that many cloudy pixels are missed.

Pure "clear sky" conservative algorithms mark pixels as cloud free or as probably cloudy, whereas pure cloud conservative algorithms detect cloudy or probably cloud free pixel. However, in practice most cloud detection algorithms try to minimize the probability of the first and second order errors in cloud and cloud free detection, only with the tendency to cloud or to clear sky conservative respectively. What cloud detection algorithm should be used is mainly a question of the consecutive algorithm. Algorithms relying on cloudy pixels need a cloud conservative detection and conversely; climatological applications often require balanced detection to be bias free [22].

MERIS measures radiances in 15 channels between 400nm and 1000nm. Thus the very valuable thermal information and information about the liquid and ice water absorption at 1.6 μ m and 3 μ m are not available. The cloud detection for MERIS therefore relies on bands (10), (11) and (12) according to Lindstrot *et al.* [17]. In addition a slight absorption of snow at 900nm could be used to discriminate snow from low clouds [13].

To perform the algorithm, the simulated MERIS bands radiance used to train the Artificial Neural Network to discriminate between the cloudy and cloud free. MOMO training datasets simulation used to conduct one of the three general atmospheric cases namely: a tropical, a, a subarctic summer and winter, and U.S. Standard Atmosphere [23]. For proper Artificial Neural Network implementation, the following inputs are needed [17]:

1. The radiance in MERIS band 10,
2. The radiance ratio *r* of MERIS band 11 (stray light corrected) and the window radiance interpolated from bands 10 and 12.
3. The aerosol optical thickness at 550nm (fixed to 0.15)
4. The cosine of the solar incident angle
5. The cosine of the viewing angle
6. The cosine of the azimuth distance (viewing azimuth – solar azimuth, 0° ≡ sensor opposite of sun) times the sinus of the viewing angle.

7. The central wavelength of MERIS band 11.

To corroborate the certainty of the produced cloud probability maps, seven flags were used to classify the MERIS imagery data according to the Table 1. The previously mentioned procedures were followed for all MERIS data sets (59 acquired MERIS images) in order to conduct the spatiotemporal final map over the designated area.

Table 1, Flags used to corroborate the cloud probability maps of MERIS imagery

Name	Value	Description
Cosmetic	1	Pixel is cosmetic
Duplicated	2	Pixel has been duplicated (filled in)
Glint_Risk	4	Pixel has glint risk
Suspect	8	Pixel is suspect
LAND and/or OCEAN	16	Pixel is overland, not ocean
Bright	32	Pixel is bright
Coastline	64	Pixel is part of a coastline
Invalid	128	Pixel is invalid

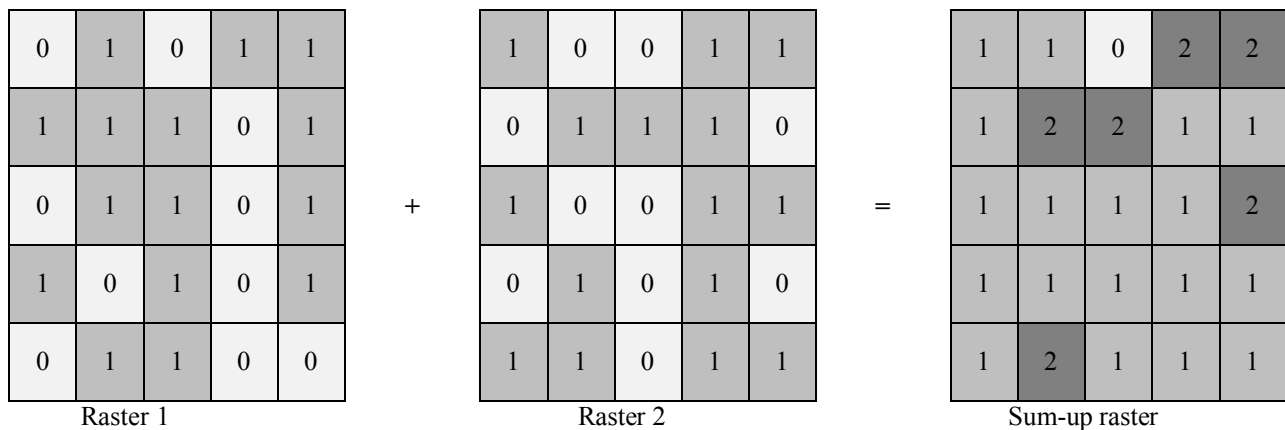
2.2.4. Cell statistics

Under GIS environments [24], cell statistics calculates a per-cell statistic from multiple rasters (59 raster), in the current case the “Sum” command which calculates the sum or all input raster values as it illustrated in Figure 3, is the used one for cell statistics. All the inputs rasters are integer; the final output is then integer and had been converted into percentages raster based on 0 and 1 cloud probability.

The final raster cloud probability map values rangers from 0 to 59 as the maximum total, 0 sum corresponded to 0% clouds and 59 corresponded to 100% clouds. Classifying the final spatiotemporal

cloud probability map was based on Jenks rule of classification, where the output classes were based on natural groupings innate in the data [24]. Jenks rule identifies break points by picking the class breaks that best group similar values and heighten the differences between classes. The features were divided into classes whose boundaries were set where there were fairly big jumps in the data values. The final output map were divided into three classes,

- a- Not cloudy
- b- Marginally cloudy and
- c- Cloudy.



Raster 1
Figure 3, Sum command illustration

3. Results and Discussion

Implementing the algorithm over the southern part of Kingdom of Saudi Arabia (Asir region) proved

accurate results that performed under the tropical atmosphere case of Artificial Neural Network implementation [17; 25]. In a more limited study of a

similar approach from March (2000), Mecikalski *et al.* [26] reported the method determined the correct sky conditions is successful by 75% of the time. Cloud probability algorithm produced cloud maps with three levels of certainty (Figure 4): A- more than 80% cloud probability (cloudy), B- from 80 to 20% cloud probability (marginally cloudy) and C- less than 20% cloud probability (not cloudy). Certainty levels were converted into three cloud probability classes as shown in Figure 5. According to table 1, most of the used flags belong to suspect pixels (value of 8) and to

overland pixels (value of 16; Figure 6) to confirm the capacity of the algorithm performance over the designated study area which is mainly an agricultural land and desert [27; 28]. There is a significant difference between cloud free water and cloudy water pixels from Figure 7. Therefore, the clear pixels could be separated from cloudy pixels if a proper threshold value was selected. However, this also indicates the discrimination between land and sea by using the image of brightness temperature is successful [29; 30].

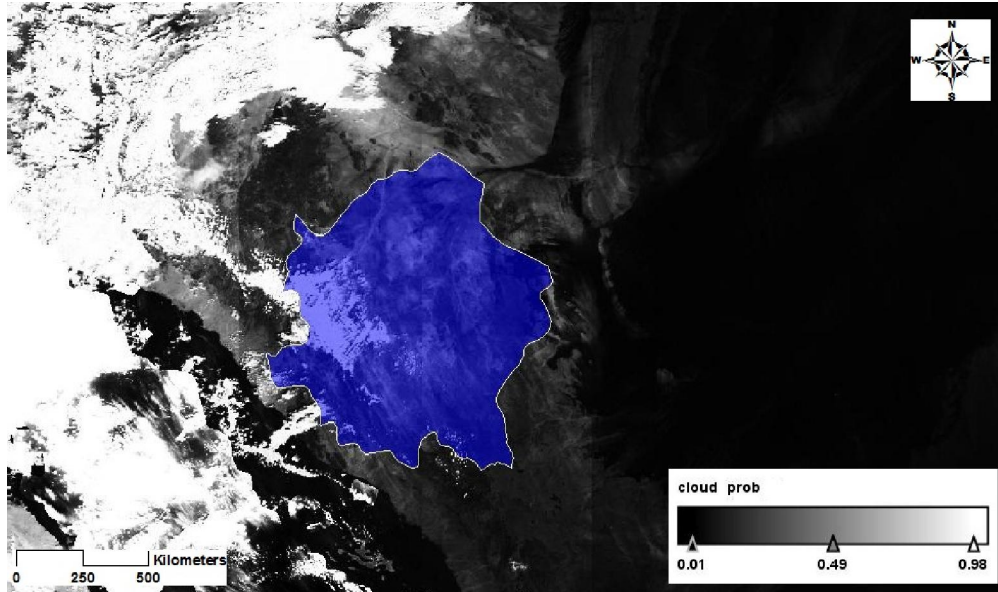


Figure 4, Cloud certainty map over the southern part of KSA

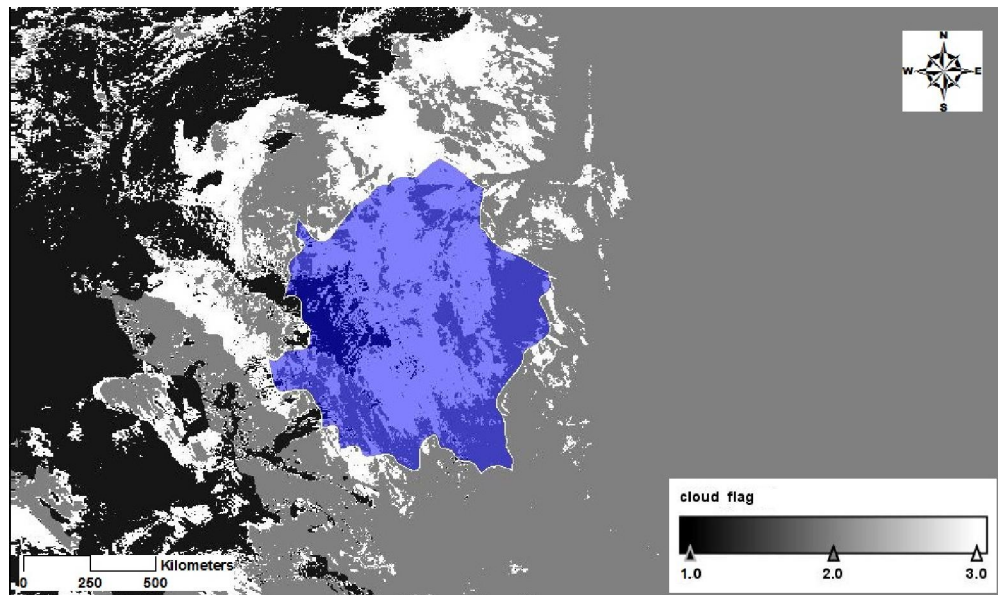


Figure 5, Cloud probability map over the southern part of KSA

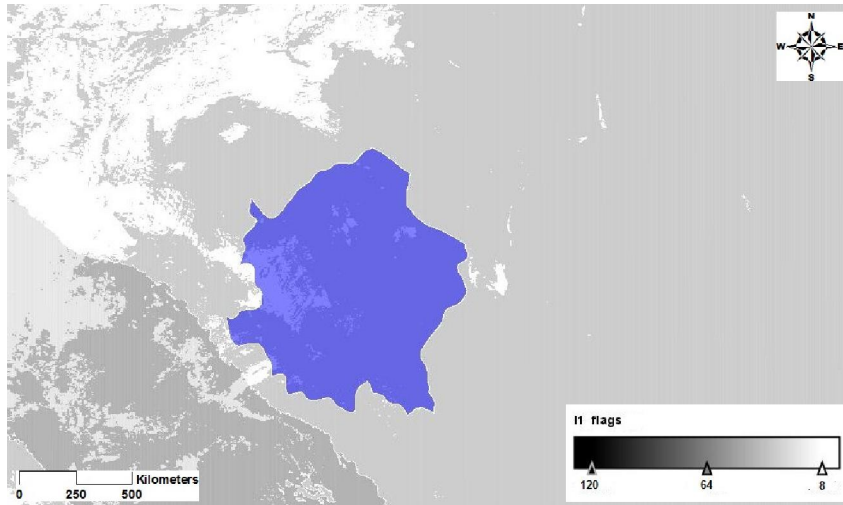


Figure 6, Cloud probability classification flags used over the Southern part of KSA

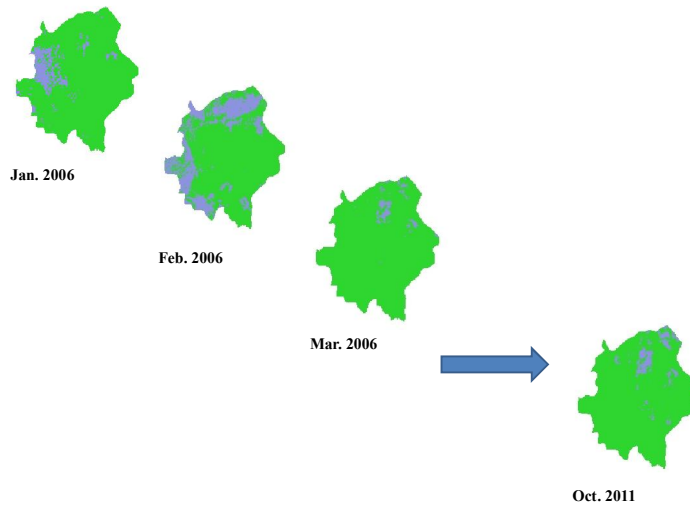


Figure 7, Cloud probability map of 59 MERIS data set of Asir region in KSA from January 2006 to October 2011

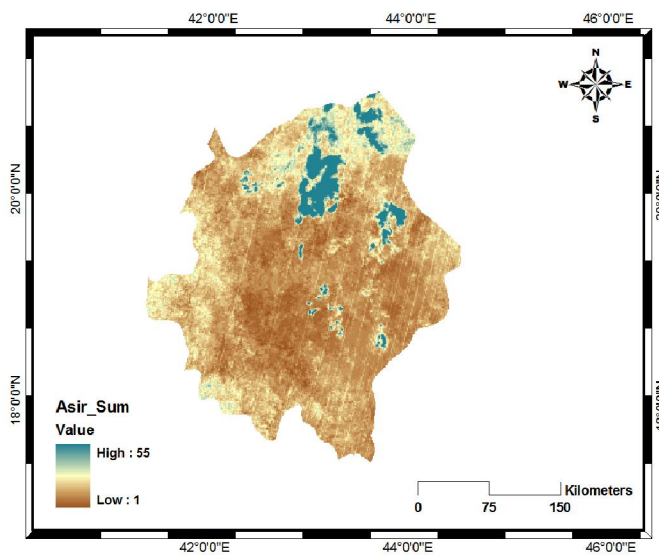


Figure 8, Total cloud probability map of Asir region in KSA from January 2006 to October 2011

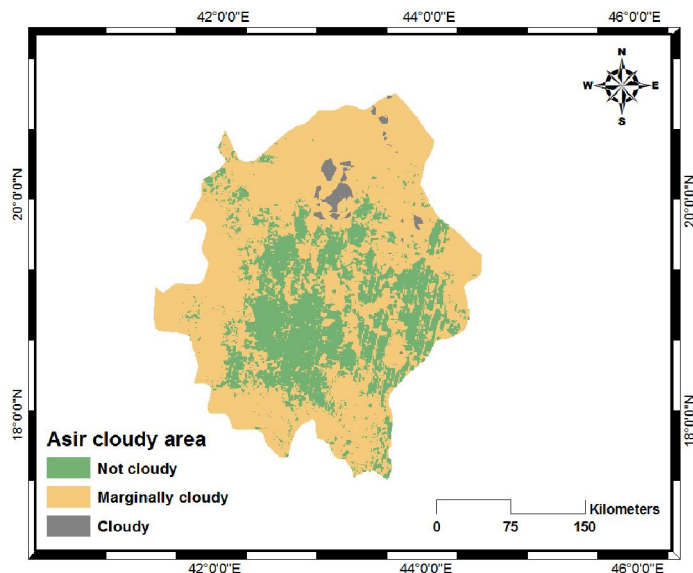


Figure 9, Spatio-Temporal distribution of the total cloud probability map of Asir region in KSA from January 2006 to October 2011

The algorithm had been applied repeatedly to the 59 data sets of MERIS data collected and processed from January 2006 till October 2011 (Figure 8) to fulfill the defined purpose of producing spatiotemporal cloud distribution map (Figure 9). Maps with more than 80% cloud certainty were only selected to be further processed under GIS environment to avoid the validation of the used technique [31; 32].

Figure 9 illustrates the spatiotemporal distribution of the clouds over Asir region for the last 5 years classified into three category according to Jenks rule as following: not cloudy area is about: 22802 km² (29.5%), marginally cloudy area is about: 53141 km² (69.0%) and cloudy area is about: 1145 km² (1.5%) of the total area Asir region (77088 km²).

It is not easy to compare different algorithm of cloud detection because the different setting and requirements of each technique. The current algorithm proved to be efficient in cloud detection over agricultural land and desert [27; 33; 34; 35].

Using different flags for cloud detection method produced qualitative and reliable results in corresponding to the infrared window channel exits in MERIS data. Frey *et al.* [31] reported that different flags indicate that different cloud flags do well in capturing the gross cloud features on this day and time. Flags capture the obvious cold clouds observed in the infrared image, but some differences exist in cloud detection for low (warm) clouds over the ocean and land regions.

According to McNally and Watts [36], an interesting feature in the Mediterranean image is a swath of what is believed to be aerosol. The scheme

has obviously reacted to the adopted method and flagged the area cloudy in correlation to the sensitivity to Saharan dust [37; 38; 39].

4. Conclusions and Recommendations

The aim of the present work is to apply the cloud probability algorithm developed by the Institute for Space Science, Free University Berlin. Performing the algorithm resulted in a robust cloud probability maps over the designated area. Classifying the resulted maps into two classes cloudy and not cloudy eases the sum of all the cloudy pixels of the 59 probability maps conducted. The spatiotemporal distribution of the clouds raises the quest for the proper use of such a method. The correlation between the cloudy pixels and land use land cover beneath is the keystone of proper practice of the current approach. As the clouds are the main source of precipitation so using the cloud probability maps will be strongly correlated to water resources management in the area. The practices of water resources management are many but the present methodology helps decision makers to decide where the dams need to be built to increase the potentials of groundwater recharge as a direct implementation of the adopted method. However, several applications of integrated water resources management or risk assessments may benefits from the current method, i.e.: estimation of soil moisture content, improvement of rainfed agriculture and/or to produce risk maps to avoid the drastic results of flooding events that may occur. Further work on the correlation between the cloud probability maps and land use land cover

beneath may need to be carried out.

Acknowledgment

This work was funded by the Deanship of Scientific Research (DSR), King Abdulaziz University, Jeddah, under grant No. (155-001-D1434). The authors, therefore, acknowledge with thanks DSR technical and financial support.

References

1. Winston, J. S. (1976). Planetary-scale characteristics of monthly mean longwave radiation and albedo and some year-to-year variations, *Mon. Weather Review*, 95: 235 - 256.
2. Stephens, G. L., Campbell, G. G., Vonder Haar, T. H. (1981). Earth radiation budgets, *Journal of Geophysics Research*, 86: 9739-9760.
3. Goodman, A.H., Henderson-Sellers, A. (1988). Cloud detection analysis: A review of recent progress. *Atmospheric Research*, 21: 203 - 221.
4. Feister, U., Gericke, K. (1998). Cloud flagging of UV spectral irradiance measurements. *Atmospheric Research*, 49(2): 115 - 138.
5. Simpson, J. (1999). Improved cloud detection and cross-calibration of ATSR, MODIS and MERIS data. In (ESA-SP-479), E. P. D., editor, ATSR International Workshop on the Applications of the ERS along track scanning radiometer.
6. Rossow, W.B. (1989). Measuring cloud properties from space: A review. *Journal of Climate*, 2: 201 - 213.
7. Rossow, W.B., Moshier, F., Kinsella, E., Arking, A., Desbois, M., Harrison, E., Minnis, P., Ruprecht, E., Seze, G., Simmer, C., Smit, E. (1985). ISCCP cloud algorithm intercomparison. *Journal of Climate and Applied Meteorology*, 24: 877 - 892.
8. Coakley, J. A., Bretherton, F. P. (1982). Cloud cover from high-resolution scanner data: Detecting and allowing for partially filled fields of view. *Journal of Geophysics Research*, 87: 4917 - 4936.
9. Tovinkere, V. R., Penalzoza, M., Logar, A., Lee, J., Weger, R. C., Berendes, T. A., Welch, R. M. (1993). An intercomparison of artificial intelligence approaches for polar scene identification. *Journal of Geophysics Research*, 98: 5001 - 5029.
10. Ebert, E.E. (1987). A pattern recognition technique for distinguishing surface and cloud types in the Polar Regions. *Journal of Climate and Applied Meteorology*, 26: 1412 - 1431.
11. Gallaudet, T. C., Simpson, J.J. (1991). Automated cloud screening of AVHRR imagery using split-and-merge clustering. *Remote Sensing of Environment*, 38: 77 - 100.
12. Elhag, M., Psilovikos, A., Sakellariou, M. (2013). Land use changes and its impacts on water resources in Nile Delta region using remote sensing techniques. *Environment, Development and Sustainability*, 15: 1189-1204.
13. Delwart, S., Preusker, R., Bourg, L., Santer, R., Ramon, D., Fischer, J. (2007). MERIS inflight spectral calibration. *International Journal of Remote Sensing*, 28: 479 - 496.
14. Brockmann, C., Ruescas, A., Stelzer, K. (2011). MERIS pixel identification. *ATBD*, 2-17, ESA-ESRIN.
15. Fischer, J., Grassl, H. (1991). Detection of cloud-top height from backscattered radiances within the oxygen A band. Part 1: Theoretical study. *Journal of Applied Meteorology*, 30: 1245-1259.
16. Fell, F., Fischer, J. (2001). Numerical simulation of the light field in the atmosphere-ocean system using the matrix-operator method. *Journal of Quantitative Spectroscopy and Radiative Transfer*, 3: 351 - 388.
17. Lindstrot, R., Preusker, R., Fischer, J. (2009). The retrieval of land surface pressure from MERIS measurements in the Oxygen A band. *American Meteorological Society*, 1367 - 1377.
18. King, M. D., Kaufman, Y. J., Menzel, W. P., Tanré, D. (1992). Remote sensing of cloud, aerosol, and water vapor properties from the Moderate Resolution Imaging Spectrometer (MODIS). *IEEE Transactions on Geoscience and Remote Sensing*, 30: 1 - 27.
19. Saunders, R. W., Kriebel, R. T. (1988). An improved method for detecting clear sky and cloudy radiances from AVHRR data. *International Journal of Remote Sensing*, 9: 123 - 150.
20. Mecikalski, J. R., Minnis, P., Palikonda, R. (2013). Use of satellite derived cloud properties to quantify growing cumulus beneath cirrus clouds. *Atmospheric Research*, 120-121: 192 - 201.
21. Mölders, N., Laube, M., Raschke, E. (1995). Evaluation of model generated cloud cover by means of satellite data. *Atmospheric Research*, 39(1-3): 91 - 111.
22. Kazantzidis, A., Tzoumanikas, P., Bais, A. F., Fotopoulos, S., Economou, G. (2012). Cloud detection and classification with the use of whole-sky ground-based images. *Atmospheric Research*, 113: 80 - 88.
23. McClatchey, R., Fenn, R., Selby, J., Volz, F., Garing, J. (1972). Optical properties of the atmosphere. 3rd ed. AFCRL-72- 0497, Environmental Research Paper 411, 108 pp.

24. ESRI (2008) ArcMap. Version 9.3 User manual. Redlands, CA, USA, pp. 135–137
25. Petty, G. W. (2006). A first course in atmospheric radiation. Sundog Publishing, 460 pp.
26. Mecikalski, J. R., Watts, D., Koenig, M. (2011). Use of Meteosat Second Generation optimal cloud analysis fields for understanding physical attributes of growing cumulus clouds. *Atmospheric Research*, 102(1-2): 175 – 190.
27. Fischer, J., Preusker, R., Schüller, L. (1997). ATBD cloud top pressure. European Space Agency Algorithm Theoretical Basis Doc. PO-TN-MEL-GS-0006, 28 pp.
28. Psilovikos, A and Elhag, M. (2013). Forecasting of Remotely Sensed Daily Evapotranspiration Data over Nile Delta Region, Egypt. *Water Resources Management*, 27(12): 4115-4130.
29. Feister, U., Möller, H., Sattler, T., Shields, J., Gørsdorf, U., Güldner, J. (2010). Comparison of macroscopic cloud data from ground-based measurements using VIS/NIR and IR instruments at Lindenberg, Germany. *Atmospheric Research*, 96: 395 – 407.
30. Guan, N. H., Zubir, M., Jafri, M., Abdullah, K. (2010). Improved cloud detection technique at South China Sea. *Aerospace Technologies Advancements*, SBN 978-953-7619-96-1, 492 pp.
31. Frey, R. A., Ackerman, S. A., Liu, Y., Strabala, K. I., Zhang, H., Key, J. R., Wang, X. (2008). Cloud detection with MODIS. Part I. Improvements in the MODIS cloud mask for collection 5. *Journal of Technology*, 25: 1057 - 1072.
32. Jedlovec, G. J., Haines, S. L., LaFontaine, F. J. (2008). Spatial and temporal varying thresholds for cloud detection in GOES imagery. *IEEE Trans. Geoscience of Remote Sensing*, 46(6): 1705 - 1717.
33. Fischer, J., Bennartz R. (1997). Retrieval of total water vapour content from MERIS measurements, Algorithm Theoretical Basis Document PO-TN-MEL-GS-0005, ESA-ESTEC, Noordwijk, Netherlands.
34. Key, E. L., Minnett, P. J., Jones, R. A. (2004). Cloud distributions over the coastal Arctic Ocean: surface-based and satellite observations. *Atmospheric Research*, 72(1-4): 57 – 88.
35. Lindstrot, R., Preusker, R., Fischer, J., (2010). The empirical correction of stray light in the MERIS oxygen A band channel, *Journal of Atmosphere and Oceanic Technology*, 27 (7): 1185 - 1194.
36. McNally, A. P., Watts, P. D. (2003). A cloud detection algorithm for high spectral resolution infrared sounders. *Quarterly Journal of the Royal Meteorological Society*, 129: 3411 - 3423.
37. Weaver, C., Ginoux, P., Hsu, C., Chou, M., Joiner, J. (2001). Radiative forcing of Saharan dust. GOCART model simulations compared with ERBE data. *Journal of the Atmospheric Sciences*, 59(3): 736 – 747.
38. Ramos, A. M., Ramos, R., Sousa, P., Trigo, R. M., Janeira, M., Prior, V. (2011). Cloud to ground lightning activity over Portugal and its association with circulation weather types. *Atmospheric Research*, 101(1-2): 84 – 101.
39. Elhag, M., Psilovikos, A. Manakos, I., Perakis, K. (2011). Application of SEBS model in estimating daily evapotranspiration and evaporative fraction from remote sensing data over Nile Delta. *Water Resources Management*, 25(11): 2731-2742.